Non-Stationary Narrowband MIMO Inter-Vehicle Channel Characterization in the 5 GHz Band

Olivier Renaudin, Veli-Matti Kolmonen, Pertti Vainikainen, and Claude Oestges

***Abstract*—In this paper, we describe measurements and models of 30×30 narrowband Multiple-Input Multiple-Output (MIMO) Vehicle-to-Vehicle (V2V) radio propagation channels at 5.3 GHz. Four environments were considered: a campus, a highway, a sub-urban area and an urban area. Since the scattering environment may change rapidly in V2V communications, we first investigate the validity of the Wide-Sense Stationarity (WSS) assumption for such channels using the Correlation Matrix Distance (CMD), which is a metric for the characterization of the MIMO channel non-stationarity. Moreover, statistical channel models were developed for these environments, which take into account the non-stationary behavior of the measured V2V channels. The large-scale fading was found to be lognormally distributed while the small-scale fading was characterized by the flexible Weibull distribution. Lastly, the non-stationary behavior of both the large-scale fading and small-scale fading statistics was investigated.**

***Index Terms*—Channel sounding, vehicular radio propagation channels, time-variant parameter estimation, channel modeling.**

I. Introduction

INTELLIGENT Transportation System (ITS) infrastructures based on mobile-to-mobile wireless communications are currently being intensively researched. Various kinds of new applications are expected for V2V communications, ranging from road traffic safety (collision avoidance, congestion prediction, etc.) to social networking and multimedia services. In V2V communication systems, vehicles can be considered as nodes in a mobile vehicular ad-hoc network, which implies that cellular wireless networks (with fixed base stations) are not required for communications between vehicles.

The IEEE 802.11p standard [1], also known as Wireless Access in Vehicular Environments (WAVE), has been recently published and is a promising technology to enable V2V communications in the 5 GHz band. The design and deployment of the IEEE 802.11p, as well as alternative V2V wireless communication systems, require a deep understanding of the underlying V2V radio propagation channel behavior. It differs significantly from that of classical cellular wireless networks because *(i):* both the transmitter (Tx) and the receiver (Rx) are mobile, *(ii):* the antennas have relatively low heights and *(iii):* the scattering environment can change very rapidly. Thus, V2V radio channels require distinct measurements and models.

O. Renaudin and C. Oestges are with the Université catholique de Louvain (UCL), Microwave Laboratory, 1348 Louvain-la-Neuve, Belgium (e-mails: olivier.renaudin@uclouvain.be, claude.oestges@uclouvain.be).

V.M. Kolmonen and P. Vainikainen are with the Aalto University SMARAD Radio Science and Engineering, PO Box 13000, FI-00076 Aalto, Finland (e-mails: velimatti.kolmonen@tkk.fi, pertti.vainikainen@tkk.fi).

Single-Input Single-Output (SISO) radio channel measurements were first conducted at a center frequency of 900 MHz between parked cars in a highway environment [2] and of 915 MHz in a mobile environment [3]. Inter-vehicle channels were also measured at 2.4 GHz in highway and urban environments [4], including joint Doppler-delay power profiles. Flat-fading narrowband channel measurements in the 5 GHz band were reported in [5], [6] in various environments. More recently, wideband V2V channel measurements were carried out at 5.12 GHz [7] and 5.9 GHz at chosen highway sites [8]. Lastly, wideband MIMO V2V channel were measured at 2.5 GHz [9] and 3.5 GHz [10] in rural environments and at 5.2 GHz in urban and highway environments [11], [12].

Most of these empirical studies include an analysis of the fading statistics. The narrowband small-scale fading was found to be Rice distributed in [5]. The small-scale fading was also characterized using the flexible Nakagami distribution [6], where its dependence on the inter-vehicle distance was highlighted, or the flexible Weibull distribution [7]. Moreover, a number of tapped-delay line models for V2V channels were reported in [7], [8], [13], [14], with relatively wide bandwidths (i.e. 5 to 20 MHz). A method to develop a channel emulator model for a doubly selective V2V wireless channel was also proposed in [8].

On the other hand, theoretical two-dimensional (2D) SISO channel models were proposed in [15], [16]. Based on them, 2D narrowband MIMO channel models were developed in [17], [18]. More recently, a three-dimensional (3D) narrowband MIMO channel model was described in [19], and was extended to 3D wideband MIMO channels [20]. This last model was validated using data collected during a measurement campaign [21]. However, the main drawback of all these models is that they are mostly based on the sum of sinusoids approach and assume an isotropic scattering around the Tx and Rx vehicles.

As a consequence, additional measurement campaigns are needed to design more accurately V2V channel models, particularly for MIMO systems. Since the scattering environment can change very rapidly in V2V communications, the Wide-Sense Stationarity (WSS) assumption remains valid only for short distances. Therefore, it is crucial to identify WSS intervals so as to estimate accurately the time-variant V2V channel statistics. The stationarity of SISO channels was investigated in [22], where local regions of stationarity were defined based on the correlation between consecutive power delay profiles. The concept of local scattering function (LSF) was introduced in [23] so as to characterize the channel non-stationarity and has already been applied in the context of V2V channels in

[24], [25]. For narrowband MIMO channels, the Correlation Matrix Distance (CMD) was introduced in [26], [27] so as to measure the variations in the spatial structure of the MIMO channel. A generalized definition of the CMD was proposed in [28] for wideband MIMO channels.

However, to the authors' knowledge, the characterization of the non-stationary V2V channel statistics is currently lacking in the literature and could be of interest to get a more in-depth understanding of the V2V channel behavior. From a practical point of view, adaptive transmission schemes that take advantage of such non-stationary statistics could then be considered. For example, the feedback rate from the Rx to the Tx could be adjusted depending on the amount of change in the spatial structure of the MIMO channel, i.e. it would be decreased (resp. increased) for large (resp. small) stationarity intervals, so that up to date estimated channel statistics would be always available at the Tx side. Moreover, it could be of interest in adaptive beamforming algorithms (i.e. the signal is transmitted in the directions providing the largest gains), which are sensitive to changes in the spatial structure of the MIMO channel [29]. Based on these observations, we carried out a measurement campaign of the MIMO V2V channel in Helsinki, Finland, in August 2007.

This paper is organized as follows: Section II contains a detailed description of the measurement campaign. Section III investigates the validity of the WSS assumption for the measured narrowband V2V channels using the CMD metric. Section IV provides narrowband V2V channel models in various environments, including the non-stationary behavior of the large-scale fading and small-scale fading. Finally, section V provides a summary and a concluding discussion.

II. Experimental Set-Up

A. Channel Sounder

For our measurements, we used the channel sounder which is available at the Helsinki University of Technology (TKK) [30]. It performs MIMO measurements at a center frequency of 5.3 GHz, that is regarded as being as close to the 5.9 GHz frequency band of the IEEE 802.11p standard such that no significant differences in channel statistics are expected. A 60 MHz measurement bandwidth was used, leading to a high delay resolution $\Delta\tau$ of 16.7 ns. The maximum transmit power was 36 dBm (i.e. 3.98 W).

The snapshot time (i.e. the time required to measure all antenna pair channels) was set at $t_{\text{snap}} = 8.4$ ms, while the macroscopic snapshot repetition rate ν_{rep} was set at 14.3 Hz to limit the recorded file sizes. The main channel sounder parameters are summarized in Table I.

TABLE I
Channel Sounder Parameters

Center frequency, f	5.3 GHz
Measurement bandwidth, BW	60 MHz
Sampling frequency, F_{s}	120 MHz
Delay resolution, $\Delta\tau = 1/BW$	16.7 ns
Transmit power, P_{Tx}	36 dBm
Snapshot time, t_{snap}	8.4 ms
Snapshot repetition rate, $\nu_{\text{rep}} = 1/t_{\text{rep}}$	14.3 Hz
Maximum resolvable Doppler shift, ν_{max}	7.15 Hz

Fig. 1. Antenna arrays used at both the Tx and Rx sides

B. Antennas

Semispherical antenna arrays were used at the Tx and Rx sides. The antenna arrays consisted of 16 dual-polarized elements (i.e. 32 feeds), which were arranged in a spherical geometry [30], as shown in Fig. 1. Polarizations were horizontal and vertical in the Rx antenna array, whereas the elements were slanted 45 degrees in the Tx antenna array.

In the Rx antenna array, the first feed was replaced with a discone antenna and the second feed was terminated and acted as a marker channel. In the Tx antenna array, the second last feed was terminated while the last feed was connected to a discone antenna and was not measured. The discone antennas were used for adjusting the Automatic Gain Control (AGC) of the channel sounder. Therefore, for further calculations, the 15 remaining antenna elements at Tx and Rx were selected in order to form the MIMO channel matrix, leading to $N_{\text{r}} \times N_{\text{t}} = 30 \times 30$ temporal multiplexed channels.

C. Vehicles and Routes

The Tx (resp. Rx) antenna array was mounted on a wooden platform on the car roofs. The antennas were covered with a plastic tarpaulin to protect them from air streams and rain.

The measurement set-up, i.e. the channel sounders, power amplifiers, batteries and laptops, were placed in the trunks of

Fig. 2. Photos of the Rx measurement vehicle (left) and of its trunk (right)

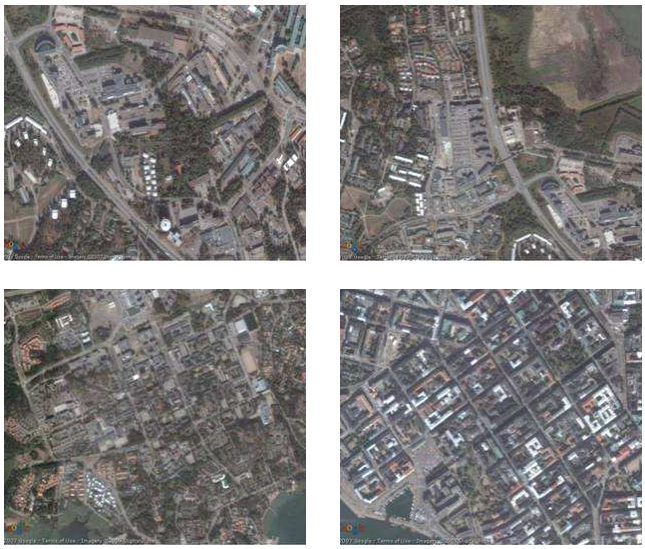

Fig. 3. Satellite photos of the environments: the campus (top left), the highway (top right), the suburban (bottom left) and urban (bottom right) areas (Pictures: Google ©)

the Tx and Rx vehicles. Fig. 2 shows the Rx vehicle employed during the measurement campaign. The Tx and Rx vehicles were always traveling in the same direction, the Tx vehicle in front of the Rx vehicle. Note that other possible scenarios (e.g. with Tx and Rx vehicles traveling in opposite directions) were not considered. Their precise positioning and speed were not available during the measurements. The vehicles' speed was in the range of 5 - 15 km/h, so that so that the channel coherence is, in the worst case, still larger than t_{snap}. The inter-vehicle distance varied between 10 and 500 m, depending on the traffic conditions and the environment.

The measurements were carried out during one afternoon in four environments: on a campus (Otaniemi), on a highway (Ring 1), in urban (Helsinki) and sub-urban (Matinkyl, Leppvaara) areas, as shown in Fig. 3. Both the campus and suburban environments are very similar, with small detached houses, parking lots and an average tree density on both sides of the streets. On the highway, the Tx and Rx vehicles were driven on the hard shoulder and were passed by other vehicles with higher speeds. The urban measurements were taken in the city center of Helsinki, with six to eight-storey buildings on both sides of the streets. Occasional blockage of the line-of-sight (LOS) occurred due to large vehicles (e.g. buses, trucks, etc.) or buildings when the Tx vehicle turned a corner.

D. Data Post-Processing

At the output of the channel sounder, we obtain the complex wideband $N_\mathrm{r} \times N_\mathrm{t} = 30 \times 30$ MIMO channel matrices

$$\mathbf{G}(\tau_k, nt_\mathrm{rep}), \tag{1}$$

where $k = 0, ..., K-1$ and $n = 0, ..., N-1$ are the delay and time indices, respectively. The narrowband complex MIMO channel matrices were obtained from these impulse responses by summation in the delay domain:

$$\mathbf{H}(nt_\mathrm{rep}) = \sum_{k=0}^{k-1} \mathbf{G}(\tau_k, nt_\mathrm{rep}). \tag{2}$$

These MIMO snapshots will be used to develop narrowband channel models in the context of V2V communications.

III. Validity of the WSS Assumption

A. Correlation Matrix Distance

The CMD was first introduced in [26] to characterize the stationarity of narrowband MIMO channels. It measures the amount of change in the structure of the correlation matrices, which are often used for statistical modeling of the MIMO channels. The CMD between two arbitrary correlation matrices $\mathbf{R}(it_\mathrm{rep})$ and $\mathbf{R}(jt_\mathrm{rep})$ is therefore defined as:

$$d_\mathrm{corr}(i,j) = 1 - \frac{\mathrm{tr}\left\{\mathbf{R}(it_\mathrm{rep})\mathbf{R}(jt_\mathrm{rep})\right\}}{\left\|\mathbf{R}(it_\mathrm{rep})\right\|_F \left\|\mathbf{R}(jt_\mathrm{rep})\right\|_F}, \tag{3}$$

where $\mathrm{tr}\{\cdot\}$ and $\|\cdot\|_F$ are the trace operator and the Frobenius norm, respectively. The CMD ranges between zero (when the correlation matrices are equal up to a scaling factor) and one (when the correlation matrices are completely uncorrelated).

In this paper, the CMD was computed using the Tx and Rx correlation matrices, which provide information on changes at the Tx and Rx sides, leading to more insight into the MIMO

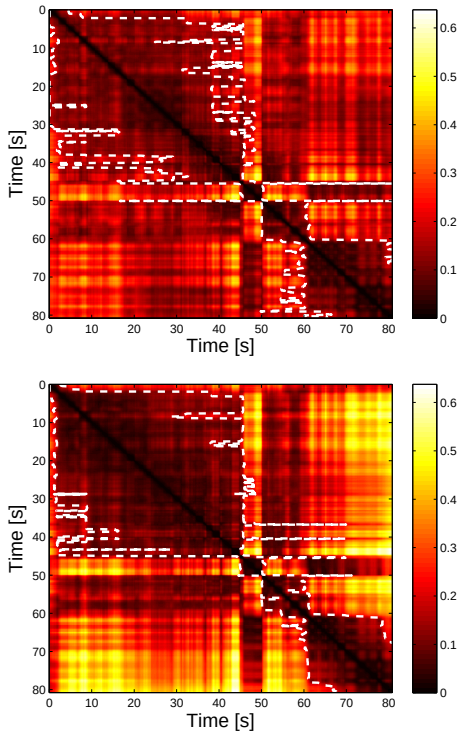

Fig. 4. Narrowband CMD estimated at both the Tx (top) and Rx (bottom) sides and the corresponding time-variant stationarity intervals {dashed} for a measurement route in the highway environment

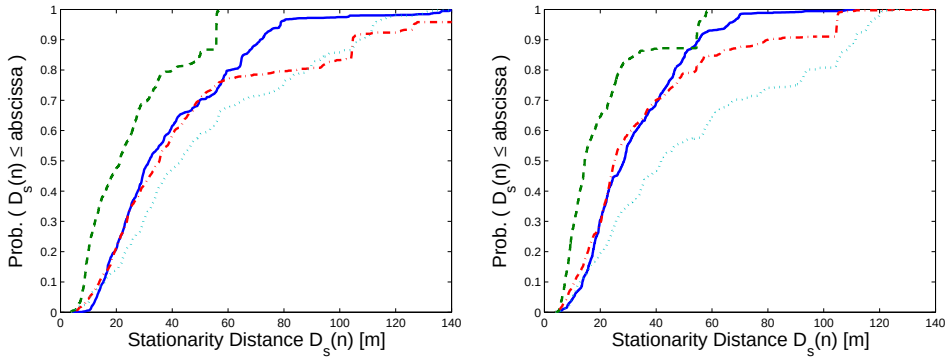

Fig. 5. CDFs of the aggregate stationarity distances at the Tx (left) and Rx (right) sides in all the environments: campus {solid}, highway {dotted}, sub-urban {dash-dotted} and urban {dashed}

radio propagation channel:

$$\hat{\mathbf{R}}_{\text{Tx}}(it_{\text{rep}}) = \frac{1}{L}\sum_{l=i}^{i+L-1} \mathbf{H}(lt_{\text{rep}})^T \mathbf{H}(lt_{\text{rep}})^*$$

$$\hat{\mathbf{R}}_{\text{Rx}}(it_{\text{rep}}) = \frac{1}{L}\sum_{l=i}^{i+L-1} \mathbf{H}(lt_{\text{rep}}) \mathbf{H}(lt_{\text{rep}})^H$$

The choice for L is not trivial, especially for fast time-varying channels, such as V2V channels [31]. Indeed, L has to be large enough to accurately estimate correlation matrices but also small enough to average over snapshots having the same statistics (i.e. the channel behavior remains unchanged over this set of snapshots). In this paper, the Tx and Rx correlation matrices were estimated using a set of $L = 25$ consecutive MIMO channel snapshots (i.e. a time period of about 1.7 s or a distance of 3.6 m, with an average vehicles' speed of $\bar{v} = 7.5$ km/h), over which the channel statistics were assumed to remain constant. This assumption will have to be further validated.

B. Estimation of the Stationarity Regions

Based on the above CMD, time-variant stationarity intervals can then be identified. Similar to [22], [24], the time-variant stationarity time $T_{\text{s}}(n)$ is defined as the maximum period over which the CMD remains below a certain threshold:

$$T_{\text{s}}(n) = \Delta n^{(n)} t_{\text{rep}}, \tag{4}$$

where $\Delta n^{(n)} = (n_{\text{max}}^{(n)} - n_{\text{min}}^{(n)})$ is the corresponding number of MIMO channel snapshots, $n = 0, ..., N - L$, and

$$\begin{cases} n_{\text{min}}^{(n)} = \underset{0 \le l \le n-1}{\arg\max}\ d_{\text{corr}}(n,l) \ge c_{\text{thresh}} \\ n_{\text{max}}^{(n)} = \underset{n+1 \le l \le N-L}{\arg\min}\ d_{\text{corr}}(n,l) \ge c_{\text{thresh}} \end{cases}$$

are the time-variant minimum and maximum bounds of the stationarity intervals $\Delta n^{(n)}$ at time nt_{rep}, respectively. The threshold was set at $c_{\text{thresh}} = 0.2$ in order to detect significant variations in the spatial structure of the MIMO channel, as reported in [27].

Fig. 4 presents a top view of the CMDs estimated between arbitrary times at the Tx and Rx sides for the given measurement route in the highway environment. It suggests that the CMDs are very similar, i.e. the spatial structure of the MIMO channel is almost the same at the Tx and Rx sides. Note that this may not always be the case, since it is highly dependent on the scattering environment in the immediate proximity of the both Tx and Rx vehicles.

TABLE II
MEAN AND STANDARD-DEVIATION OF THE LOGNORMAL DISTRIBUTION OF THE STATIONARITY INTERVALS IN ALL THE ENVIRONMENTS

	At the Tx side		At the Rx side	
	μ_{s} [in m]	σ_{s} [in m]	μ_{s} [in m]	σ_{s} [in m]
Campus	3.51	0.60	3.32	0.56
Highway	3.73	0.73	3.71	0.78
Sub-urban	3.59	0.77	3.32	0.73
Urban	3.00	0.68	2.79	0.65

Moreover, the time-variant stationarity intervals given by Eq. (4) were found to be easily identified. They are regions where the spatial structure of the MIMO channel is relatively constant. Beyond these stationarity intervals, significant variations in the spatial structure of the MIMO channel can be observed, and correspond either to non-stationarity (i.e. the CMD exceeds the threshold) or, interestingly, to other stationarity (i.e. the CMD remains below the threshold) regions.

Since stationarity times depend on the measurement vehicles' speed, we will prefer expressing stationarity distances that can be defined as

$$D_{\text{s}}(n) = v(n) T_{\text{s}}(n), \tag{5}$$

where $v(n)$ is the speed of the vehicles at time nt_{rep}. However, since the exact vehicles' speed was not available, $v(n)$ was replaced in the previous relationship by its average $\bar{v}$. Depending on the value chosen for $\bar{v}$, significant deviations of the estimated stationarity distances from the determined stationarity times may be expected and are given by

$$\Delta D_{\text{s}}(n) = \frac{\Delta \bar{v}}{\bar{v}} D_{\text{s}}(n),$$

where $\Delta \bar{v}$ and $\Delta D_{\text{s}}(n)$ are the deviations of both the average vehicles' speed and of the estimated stationarity distances, respectively. Fig. 5 provides the cumulative density functions (CDFs) of the aggregate time-variant stationarity distances

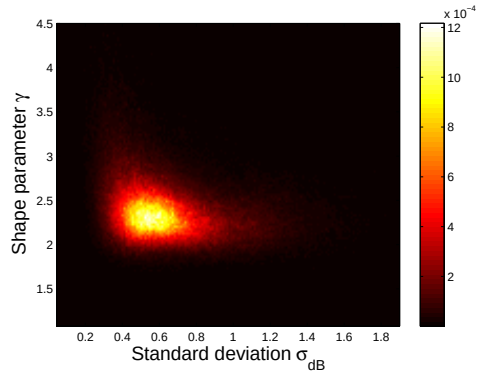

Fig. 6. Joint PDF of the shape parameter γ and the standard deviation σ_{dB} in the campus environment

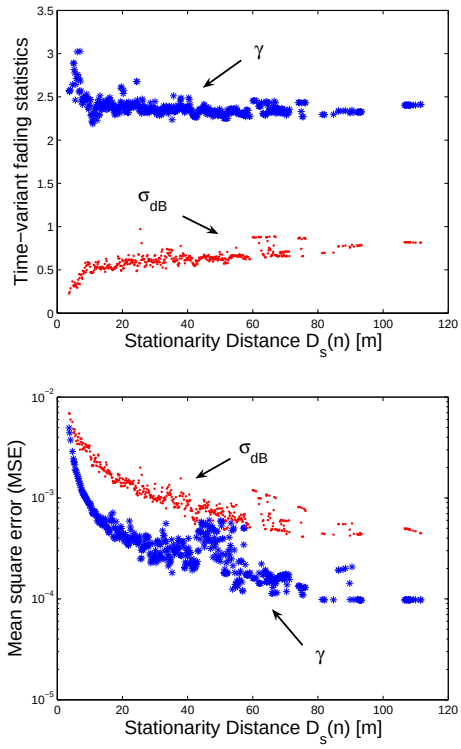

Fig. 7. Impact of the stationarity intervals on the estimation of both the median fading statistics (top) and the median goodness-of-fit (bottom) in the campus environment

estimated at the Tx and Rx sides in all the environments. When Tx and Rx vehicles are driven in the same direction with an average speed $\bar{v} = 7.5$ km/h, median stationarity distances were found to range from 10 to 40 m (note also that average vehicles' speed deviations $\Delta\bar{v}$ between -2.5 and 7.5 km/h correspond to deviations of the stationarity distances $\Delta D_{\text{s}}(n)$ ranging from $D_{\text{s}}(n)/3$ to $2D_{\text{s}}(n)$, respectively). The shortest stationarity distances were found in the urban environment, mostly due to its high density of scatterers. On the other hand, the highway environment provides the longest stationarity distances, due to a few number of scatterers and a nearly "homogeneous" scattering environment. Similar observations have been reported in [24]. Very comparable stationarity distances were found in both the campus and sub-urban environments. Interestingly, there is also no significant difference between the stationarity distances estimated at both the Tx and Rx sides in all the environments. Reason for this is that both the Tx and Rx vehicles were driven in the same direction during the measurements and were thus almost always experiencing the same scattering environment.

The stationarity distances were found to be best fitted using a lognormal distribution as reported in [22], whose Probability Density Function (PDF) is defined as:

$$f\left(r;\mu_{\text{s}},\sigma_{\text{s}}\right) = \frac{1}{\sqrt{2\pi}\sigma_{\text{s}} r}\exp\left[-\frac{\left(\ln r-\mu_{\text{s}}\right)^2}{2\sigma_{\text{s}}^2}\right], \qquad (6)$$

where μ_{s} and σ_{s} are the mean and the standard-deviation of $\ln r$, respectively. The parameters of the lognormal distributions at both the Tx and Rx sides in all the environments are summarized in Table II.

IV. Narrowband MIMO Channel Models

Based on the stationarity intervals estimated at the Rx side in the previous section, time-variant narrowband V2V channel models can be developed in various environments and could be used, for example, in adaptive transmission schemes.

A. Extraction Procedure

The time-variant large-scale fading was extracted over each stationarity interval by averaging (in power) the MIMO snapshots using a 40 wavelength sliding window (i.e. $M = 14$ snapshots) in order to remove the small-scale fading [32]:

$$\mathbf{LS}^{(n,m)} = \sqrt{\frac{1}{M}\sum_{m'=m-M/2}^{m+M/2+1}\left|\left|\mathbf{H}(m' t_{\text{rep}})\right|\right|^2}, \qquad (7)$$

where $m = n_{\text{min}}^{(n)} + M/2, ..., n_{\text{max}}^{(n)} - M/2$ are the indices of the snapshots that were used to estimate the time-variant large-scale fading over the n^{th} stationarity interval. The time-variant small-scale fading was then extracted by removing the large-scale fading from the measured data:

$$\mathbf{SS}^{(n,m)} = \frac{\left[\ \left|\mathbf{H}(m t_{\text{rep}})\right|\ \right]}{\left[\ \mathbf{LS}^{(n,m)}\ \right]}, \qquad (8)$$

which corresponds to the Hadamard division (or element-wise division) of the matrices $|\mathbf{H}(mt_{\text{rep}})|$ and $\mathbf{LS}^{(n,m)}$. In the following, we use the notation $\mathbf{LS}^{(n)}$ to denote the large-scale fading estimated over the n^{th} stationarity interval, i.e.

$$\mathbf{LS}^{(n)} = \left\{\mathbf{LS}^{(n,m)}, m = n_{\text{min}}^{(n)} + M/2, ..., n_{\text{max}}^{(n)} - M/2\right\}.$$

Similarly, $\mathbf{SS}^{(n)}$ will represent the small-scale fading estimated over the n^{th} stationarity interval. Both the large-scale fading and the small-scale fading were estimated in all the measurement routes in the environments described above.

B. Fading Analysis over Stationarity Intervals

The large-scale fading $\mathbf{LS}^{(n,m)}$ was first converted into decibels (dBs) and was found to be best fitted by a normal

distribution with zero-mean and standard-deviation σ_{dB}, in agreement with the literature. On the other hand, the small-scale fading $\mathbf{SS}^{(n,m)}$ was modeled using the flexible Weibull distribution, whose PDF is defined as:

$$f\left(r;\alpha,\gamma\right)=\frac{\gamma}{\alpha^{\gamma}}r^{\gamma-1}\exp\left[-\left(\frac{r}{\alpha}\right)^{\gamma}\right], \tag{9}$$

where $\alpha>0$ is the scale parameter and $\gamma>0$ the shape parameter. Parameter values $\gamma=2$ imply the well-known Rayleigh distributions, while $\gamma\geq 2$ (resp. $\gamma\leq 2$) yield Rician (resp. worse than Rayleigh) distributions. However, the Weibull distribution has no physical interpretation (contrary to the Rayleigh and Rician distributions) [33]. In the following, ${\sigma_{\text{dB}}}^{(n,u,v)}$ and $\gamma^{(n,u,v)}$ will refer to the standard deviation of the normal large-scale fading fit and the shape parameter of the Weibull small-scale fading fit estimated over the n^{th} stationarity interval for the (u,v) antenna pair.

The goodness-of-fit was estimated for the large-scale fading and the small-scale fading in the Mean Square Error (MSE) sense:

$$\text{MSE}=\text{E}\left[\left(F(x)-F'(x)\right)^{2}\right], \tag{10}$$

where $F(x)$ is the theoretical normal (resp. Weibull) CDF and $F'(x)$ the empirical CDF of the large-scale (resp. small-scale) fading, respectively.

Fig. 6 shows the joint PDF of the shape parameter γ and the standard-deviation σ_{dB} taken over all stationarity intervals n and all antenna pairs (u,v) in the campus environment. In this case, the small-scale fading is found to be mostly Rician distributed (with γ ranging from 2.2 up to 4.5) and thus corresponds to low levels of the large-scale fading. On the other hand, the small-scale fading can also be Rayleigh or worse than Rayleigh distributed (with γ ranging from 1.7 up to 2.2) and corresponds, as expected, to greater degrees of the large-scale fading.

Fig. 7 shows the impact of the stationarity interval length on the estimation of both the median large-scale fading and small-scale fading statistics in the campus environment. Small stationarity intervals correspond to both small σ_{dB} and large γ median values. As expected, they are associated with large MSE values, since only few snapshots were used to (inaccurately) estimate the fading statistics. On the other hand, larger stationarity intervals correspond to both larger σ_{dB} and smaller γ median values. They are associated with smaller MSE values, as the number of snapshots used to estimate the fading statistics progressively increases.

C. Non-Stationary Fading Modeling

The non-stationary behavior of ${\sigma_{\text{dB}}}^{(n,u,v)}$ for the antenna pair (u,v) was defined as:

$${\sigma_{\text{dB}}}^{(u,v)}=\left\{{\sigma_{\text{dB}}}^{(n,u,v)},n=0,...,N-L\right\}.$$

Similarly, $\gamma^{(u,v)}$ will correspond to the non-stationary behavior of $\gamma^{(n,u,v)}$ for the antenna pair (u,v).

As can be shown in Fig. 8, the variation of the statistical parameters σ_{dB} and γ between different stationarity intervals

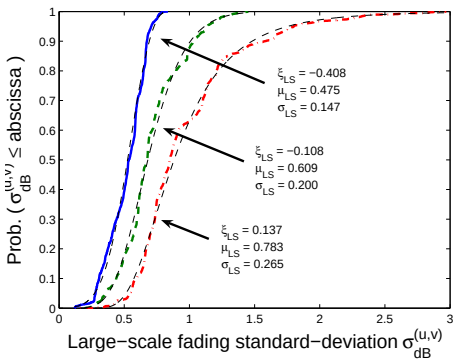

Fig. 8. Comparison between experimental CDFs of ${\sigma_{\text{dB}}}^{(u,v)}$ and theoretical GEV fits for three antenna pairs in the campus environment

can be modeled for each antenna pair using the Generalized Extreme Value (GEV) distribution, whose PDF is defined as:

$$f(x;\xi,\mu,\sigma)=\exp\left\{-\left[1+\xi\left(\frac{x-\mu}{\sigma}\right)^{-1/\xi}\right]\right\}, \tag{11}$$

where $\xi\in\mathbb{R}$ is the shape parameter, $\mu\in\mathbb{R}$ the location parameter and $\sigma>0$ the scale parameter. The value of ξ determines the nature of the GEV distribution: $\xi=0$ is associated with the light-tailed Gumbel distribution class, $\xi>0$ with the heavy-tailed Fréchet distribution class and $\xi<0$ with the Weibull distribution class (with a bounded upper tail). Owing to these three parameters, the GEV distribution is often used to model rare phenomena, e.g. in climatology, finance, etc.

In the following, $\xi_{\mathbf{LS}}$, $\mu_{\mathbf{LS}}$ and $\sigma_{\mathbf{LS}}$ (resp. $\xi_{\mathbf{SS}}$, $\mu_{\mathbf{SS}}$ and $\sigma_{\mathbf{SS}}$) will refer to the $N_{\text{r}}\times N_{\text{t}}$ matrices containing the shape, location and scale parameters of GEV fits of the large-scale fading (resp. small-scale fading) statistics, respectively.

D. Non-Stationary Fading vs. Antenna Location

Since the antenna arrays at both the Tx and Rx sides were semi-spherical with elements pointing in different directions, the fading behavior may vary from one antenna pair to another. The spatial distribution of the GEV fit parameters was taken over all the antenna pairs (u,v) and was modeled using Multi-Variate Gaussian (MVG) distributions, which are defined as:

$$f(\omega_i,\mu_i,\sigma_i)=\sum_{i=1}^{M}\omega_i\mathcal{N}\left(\mu_i,\sigma_i\right), \tag{12}$$

where $\mathcal{N}\left(\mu_i,\sigma_i\right)$ denotes the normal probability density function (PDF) of the i^{th} mode of the distribution, with mean μ_i and standard deviation σ_i, and ω_i the associated weight.

Table III provides the parameters of the MVG fits of both the shape parameters $\xi_{\mathbf{LS}}$ and $\xi_{\mathbf{SS}}$. The spatial distribution of the shape parameter $\xi_{\mathbf{LS}}$ was found to consist in two roughly equivalent modes (i.e. with associated weights $\omega_i\approx 0.5$). They are associated with either light-tailed or upper-bounded distributions of the large-scale fading statistics (i.e. $\xi_{\mathbf{LS}}\leq 0$ or, equivalently, $\mu_i\leq 0$). Thus, it means that the antenna pairs that hardly ever experience extreme large-scale fading conditions (i.e. with rare large σ_{dB} values). On the other hand, the spatial distribution of the shape parameter $\xi_{\mathbf{SS}}$ consists in only one

TABLE III
PARAMETERS OF THE MULTIVARIATE GAUSSIAN FITS OF THE GEV SHAPE PARAMETERS $\xi_{\mathbf{LS}}$ (TOP LEFT), $\xi_{\mathbf{SS}}$ (BOTTOM LEFT) AND LOCATION PARAMETERS $\mu_{\mathbf{LS}}$ (TOP RIGHT), $\mu_{\mathbf{SS}}$ (BOTTOM RIGHT)

	$i=1$ $(\omega_1,\ \mu_1,\ \sigma_1)$	$i=2$ $(\omega_2,\ \mu_2,\ \sigma_2)$
Campus	(0.41, -0.20, 0.008)	(0.59, 0.03, 0.007)
Highway	(0.46, -0.09, 0.005)	(0.54, 0.06, 0.003)
Sub-urban	(0.59, -0.11, 0.004)	(0.41, -0.04, 0.005)
Urban	(0.59, -0.09, 0.007)	(0.41, 0.16, 0.008)

	$i=1$ $(\omega_1,\ \mu_1,\ \sigma_1)$	$i=2$ $(\omega_2,\ \mu_2,\ \sigma_2)$	$i=3$ $(\omega_3,\ \mu_3,\ \sigma_3)$
Campus	(0.53, 0.49, 0.001)	(0.36, 0.61, 0.003)	(0.11, 0.82, 0.008)
Highway	(0.53, 0.54, 0.002)	(0.31, 0.66, 0.004)	(0.16, 0.86, 0.008)
Sub-urban	(0.55, 0.57, 0.003)	(0.30, 0.75, 0.007)	(0.15, 1.02, 0.013)
Urban	(0.50, 0.45, 0.003)	(0.34, 0.62, 0.006)	(0.16, 0.89, 0.009)

	$i=1$ $(\omega_1,\ \mu_1,\ \sigma_1)$
Campus	(1.00, 0.02, 0.100)
Highway	(1.00, 0.09, 0.120)
Sub-urban	(1.00, 0.03, 0.110)
Urban	(1.00, -0.03, 0.100)

	$i=1$ $(\omega_1,\ \mu_1,\ \sigma_1)$	$i=2$ $(\omega_2,\ \mu_2,\ \sigma_2)$	$i=3$ $(\omega_3,\ \mu_3,\ \sigma_3)$
Campus	(0.47, 2.21, 0.004)	(0.51, 2.34, 0.007)	(0.02, 2.79, 0.009)
Highway	(0.58, 2.16, 0.002)	(0.28, 2.21, 0.002)	(0.14, 2.62, 0.050)
Sub-urban	(0.56, 2.13, 0.003)	(0.31, 2.16, 0.003)	(0.13, 2.76, 0.101)
Urban	(0.55, 2.16, 0.008)	(0.42, 2.28, 0.015)	(0.03, 2.80, 0.042)

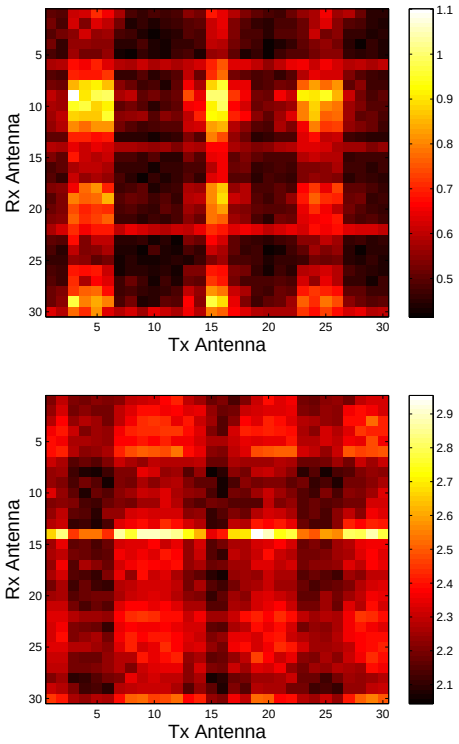

Fig. 9. Location parameters $\mu_{\mathbf{LS}}$ (top) and $\mu_{\mathbf{SS}}$ (bottom) estimated for each antenna pair in the campus environment

mode, which corresponds to light-tailed distributions of the small-scale fading statistics (i.e. $\xi_{\mathbf{SS}} \approx 0$ or, equivalently, $\mu_i \approx 0$). As a consequence, pure Rician conditions are rarely encountered, whatever the considered antenna pair.

Table III also summarizes the parameters of the MVG fits of both the location parameter $\mu_{\mathbf{LS}}$ and $\mu_{\mathbf{SS}}$. Their spatial distributions consist in three modes, each of them being associated with a different large-scale (resp. small-scale) fading level. Moreover, Fig. 9 shows that they are related to different clusters of antenna pairs. Small ${\sigma_{\text{dB}}}^{(u,v)}$ values (i.e. small μ_{LS} values) are indeed obtained for antenna pairs hidden one from the other, i.e. with Tx (resp. Rx) antennas at the front (resp. back) of the antenna arrays. This can be explained by the fact that, for such antenna pairs, the amplitude of the narrowband channel remains roughly constant over time. Hence, there is no significant variation in the extracted large-scale fading. On the other hand, larger ${\sigma_{\text{dB}}}^{(u,v)}$ values are achieved for antenna pairs facing each other, i.e. with Tx (resp. Rx) antennas at the back (resp. front) of the antenna arrays. These antenna pairs may indeed be much more impacted by shadowing, corresponding therefore to larger variations in the time-variant behavior of the large-scale fading. Quite naturally, note also that ${\sigma_{\text{dB}}}^{(u,v)}$ is strongly anti-correlated with $\gamma^{(u,v)}$ (i.e. μ_{LS} are μ_{SS} are strongly anti-correlated).

TABLE IV
CROSS-CORRELATION BETWEEN THE GEV FIT PARAMETERS OF BOTH THE LARGE-SCALE FADING AND THE SMALL-SCALE FADING

	$\langle \xi_{\mathbf{LS}}, \mu_{\mathbf{LS}} \rangle$	$\langle \mu_{\mathbf{LS}}, \sigma_{\mathbf{LS}} \rangle$	$\langle \xi_{\mathbf{SS}}, \mu_{\mathbf{SS}} \rangle$	$\langle \mu_{\mathbf{SS}}, \sigma_{\mathbf{SS}} \rangle$
Campus	0.44	0.92	0.29	0.76
Highway	0.04	0.92	-0.38	0.90
Sub-urban	-0.16	0.95	-0.46	0.91
Urban	-0.66	0.95	-0.04	0.85

Table IV provides the cross-correlation coefficients between the GEV fit parameters in all the environments. As it can be observed, there is no clear dependence of the shape parameter $\xi_{\mathbf{LS}}$ (resp. $\xi_{\mathbf{SS}}$) toward the location parameter $\mu_{\mathbf{LS}}$ (resp. $\mu_{\mathbf{SS}}$). Moreover, the scale parameter $\sigma_{\mathbf{LS}}$ (resp. $\sigma_{\mathbf{SS}}$) is highly correlated with the location parameter $\mu_{\mathbf{LS}}$ (resp. $\mu_{\mathbf{SS}}$), which can therefore be modeled based on the above analysis.

V. CONCLUSION

In this paper, we have presented results based on a V2V measurement campaign of wideband MIMO radio propagation channels in the 5 GHz band. Measurements were made in various environments (campus, highway, urban and sub-urban) in the area of Helsinki, Finland. The measured wideband data were then summed in the delay domain, in order to obtain narrowband V2V MIMO channels.

The validity of the WSS assumption for narrowband MIMO V2V channels was first investigated, by using the narrowband CMD. The stationarity distances were found in all the environments to be lognormally distributed. With vehicles driving in the same direction with an average speed of 7.5 km/h, the median stationarity distances were found to range between 10 and 40 m when estimated at both the Tx and Rx sides.

Non-stationary narrowband MIMO channels were then characterized. The large-scale fading (resp. small-scale fading) was extracted over stationarity intervals estimated at the Rx side and was found to be normal (resp. Weibull) distributed. Non-stationary fading statistics were obtained for the large-scale fading and the small-scale fading, thus providing a faithful representation of the fading conditions at any given time.

Finally, the GEV distribution was used to describe for each antenna pair the non-stationary behavior of the large-scale fading and the small-scale fading statistics. The distribution of the GEV parameters over all the antenna pairs was modeled using multivariate Gaussian distributions, whose different modes can be associated with different clusters of antenna pairs.

ACKNOWLEDGMENT

This work was carried out in the framework of COST Action 2100. The authors would like to thank Katsuyuki Haneda, Jukka Koivunen and Mikko Olkkonen for their participation in the measurement campaign, as well as the Belgian Fonds de la Recherche Scientifique and the SMARAD Centre of Excellence funding of the Academy of Finland for their financial support.

REFERENCES

[1] 802.11p, "Draft amendment to wireless LAN medium access control (MAC) and physical layer (PHY) specifications: Wireless access in vehicular environments," *IEEE P802.11p/D0.26*, January 2006.

[2] J. S. Davis and J. P. M. G. Linnartz, "Vehicle to vehicle RF propagation measurements," *28th Asilomar Conference on Signals, Systems and Computers*, vol. 1, pp. 470 – 474, October 1994.

[3] R. J. Punnoose, P. V. Nikitin, J. Broch, and D. D. Stancil, "Optimizing wireless network protocols using real-time predictive propagation modeling," *IEEE Radio and Wireless Conference (RAWCON)*, pp. 39 – 44, August 1999.

[4] G. Acosta, K. Tokuda, and M. A. Ingram, "Measured joint Doppler-delay power profiles for vehicle-to-vehicle communications at 2.4 GHz," *IEEE Global Telecommunications Conference (GLOBECOM)*, vol. 6, pp. 3813 – 3817, November 2004.

[5] J. Maurer, T. Fügen, and W. Wiesbeck, "Narrow-band measurement and analysis of the inter-vehicle transmission channel at 5.2 GHz," *IEEE 55th Vehicular Technology Conference (VTC)*, vol. 3, pp. 1274 – 1278, 2002.

[6] L. Cheng, B. E. Henty, D. D. Stancil, F. Bai, and P. Mudalige, "Mobile vehicle-to-vehicle narrow-band channel measurement and characterization of the 5.9 GHz Dedicated Short Range Communication (DSRC) frequency band," *IEEE Journal on Selected Areas in Communications*, vol. 25, no. 8, pp. 1501 – 1516, October 2007.

[7] I. Sen and D. W. Matolak, "Vehicle-vehicle channel models for the 5 GHz band," *IEEE Transactions on Intelligent Transportation Systems*, vol. 9, no. 2, pp. 235 – 245, June 2008.

[8] G. Acosta-Marum and M. A. Ingram, "Doubly selective vehicle-to-vehicle channel measurements and modeling at 5.9 GHz," *Wireless Personal Multimedia Communications Conference (WPMC)*, September 2006.

[9] J. Ling, D. Chizhik, D. Samardzija, and R. A. Valenzuela, "Peer-to-peer MIMO radio channel measurements in a rural area," *IEEE Transactions on Wireless Communications*, vol. 6, no. 9, pp. 3229 – 3237, September 2007.

[10] P. C. F. Eggers, T. W. C. Brown, K. Olesen, and G. F. Pedersen, "Assessment of capacity support and scattering in experimental high speed vehicle to vehicle MIMO links," *IEEE 65th Vehicular Technology Conference (VTC)*, pp. 466 – 470, April 2007.

[11] A. Paier, J. Karedal, N. Czink, H. Hofstetter, C. Dumard, T. Zemen, F. Tufvesson, C. F. Mecklenbräuker, and A. F. Molisch, "First results from car-to-car and car-to-infrastructure radio channel measurements at 5.2 GHz," *IEEE 18th International Symposium on Personal, Indoor and Mobile Radio Communications (PIMRC)*, pp. 1 – 5, September 2007.

[12] A. Paier, J. Karedal, N. Czink, H. Hofstetter, C. Dumard, T. Zemen, F. Tufvesson, A. F. Molisch, and C. F. Mecklenbräuker, "Car-to-car radio channel measurements at 5 GHz: Pathloss, power-delay profile and delay-Doppler spectrum," *IEEE International Symposium on Wireless Communication Systems (ISWCS)*, pp. 224 – 228, October 2007.

[13] G. Acosta-Marum and M. A. Ingram, "A BER-based partitioned model for a 2.4 GHz vehicle-to-vehicle expressway channel," *Wireless Personal Communications*, vol. 37, pp. 421 – 443, May 2006.

[14] A. Paier, J. Karedal, N. Czink, C. Dumard, T. Zemen, F. Tufvesson, C. F. Mecklenbräuker, and A. F. Molisch, "Comparison of Lund'07 vehicular channel measurements with the IEEE 802.11p channel model, td(08)436," *Proceedings 4th COST2100 Management Committee Meeting, Wroclaw (Poland)*, February 2008.

[15] A. S. Akki, "Statistical properties of mobile-to-mobile land communication channels," *IEEE Transactions on Vehicular Technology*, vol. 43, no. 4, pp. 826 – 831, November 1994.

[16] R. Wang and D. Cox, "Channel modeling for ad hoc mobile wireless networks," *IEEE 55th Vehicular Technology Conference (VTC)*, vol. 1, pp. 21 – 25, May 2002.

[17] M. Pätzold, B. Hogstad, N. Youssef, and D. Kim, "A MIMO mobile-to-mobile channel model: Part I - The reference model," *IEEE International Symposium on Personal, Indoor and Mobile Radio Communications (PIMRC)*, pp. 573 – 578, September 2005.

[18] B. Hogstad, M. Pätzold, N. Youssef, and D. Kim, "A MIMO mobile-to-mobile channel model: Part II - The simulation model," *IEEE International Symposium on Personal, Indoor and Mobile Radio Communications (PIMRC)*, pp. 562 – 567, September 2005.

[19] A. G. Zajić and G. L. Stüber, "A three-dimensional MIMO mobile-to-mobile channel model," *IEEE Wireless Communications and Networking Conference (WCNC)*, pp. 1883 – 1887, March 2007.

[20] ——, "A three-dimensional parametric model for wideband MIMO mobile-to-mobile channels," *IEEE Global Telecommunications Conference (GLOBECOM)*, pp. 3760 – 3764, November 2007.

[21] A. G. Zajić, G. L. Stüber, T. G. Pratt, and S. T. Nguyen, "Wideband MIMO mobile-to-mobile channels: Geometry-based statistical modeling with experimental validation," *IEEE Transactions on Vehicular Technology*, vol. 58, no. 2, pp. 517 – 534, February 2009.

[22] A. Gehring, M. Steinbauer, I. Gaspard, and M. Grigat, "Empirical channel stationarity in urban environments," *4th European Personal Mobile Communications Conference (EPMCC)*, February 2001.

[23] G. Matz, "On non-WSSUS wireless fading channels," *IEEE Transactions on Wireless Communications*, vol. 4, no. 5, pp. 2465 – 2478, September 2005.

[24] A. Paier, T. Zemen, L. Bernadó, G. Matz, J. Karedal, N. Czink, C. Dumard, F. Tufvesson, A. F. Molisch, and C. F. Mecklenbräuker, "Non-WSSUS vehicular channel characterization in highway and urban scenarios at 5.2 GHz using the local scattering function," *International ITG Workshop on Smart Antennas (WSA)*, pp. 9 – 15, February 2008.

[25] L. Bernadó, T. Zemen, A. Paier, G. Matz, J. Karedal, N. Czink, C. Dumard, F. Tufvesson, M. Hagenauer, A. F. Molisch, and C. F. Mecklenbräuker, "Non-WSSUS vehicular channel characterization at 5.2 GHz - Spectral divergence and time-variant coherence parameters," *XXIX General Assembly of the International Union of Radio Science (URSI)*, August 2008.

[26] M. Herdin, N. Czink, H. Özcelik, and E. Bonek, "Correlation matrix distance, a meaningful measure for evaluation of non-stationary MIMO channels," *IEEE 61st Vehicular Technology Conference (VTC)*, vol. 1, pp. 136 – 140, June 2005.

[27] M. Herdin and E. Bonek, "A MIMO correlation matrix based for characterizing non-stationarity," *13th IST Mobile and Wireless Communications Summit, Lyon (France)*, June 2004.

[28] H. Xiao and A. G. Burr, "Full channel correlation matrix of a time-variant wideband spatial channel model," *IEEE International Symposium on Personal, Indoor and Mobile Radio Communications (PIMRC)*, pp. 1 – 5, September 2006.

[29] M. Herdin, "Non-stationary indoor MIMO channels," Ph.D. dissertation, Technischen Universität Wien, 2004.

[30] V. M. Kolmonen, J. Kivinen, L. Vuokko, and P. Vainikainen, "5.3-GHz MIMO radio channel sounder," *IEEE Transactions on Instrumentation and Measurement*, vol. 55, no. 4, pp. 1263–1269, August 2006.

[31] O. Renaudin, V. M. Kolmonen, P. Vainikainen, and C. Oestges, "Impact of the correlation matrix estimation accuracy on the computation of stationarity intervals," *4th European Conference on Antennas and Propagation (EuCAP)*, Submitted.

[32] W. C. Y. Lee, "Estimate of local average power of a mobile radio channel," *IEEE Transactions on Vehicular Technology*, vol. 34, no. 1, pp. 22– 27, February 1985.

[33] I. Sen, D. W. Matolak, and W. Xiong, "Wireless channels that exhibit 'worse than Rayleigh' fading: Analytical and measurement results," *IEEE Military Communications Conference (MILCOM)*, pp. 1 – 7, October 2006.

Olivier Renaudin received in 2006 the diploma of engineer in telecommunications from the Ecole Nationale Supérieure d'Electronique, Informatique et Radiocommunications de Bordeaux and the M.Sc. degree in signal processing from the University of Bordeaux I, France. In February 2007, he joined the Microwave Laboratory at the Université catholique de Louvain (UCL), where is currently working on his doctoral thesis. His research interests are channel sounding and channel modeling for vehicular communication networks.

Veli-Matti Kolmonen received his M.Sc. degree in technology from Helsinki University of Technology (TKK), Espoo, Finland, in 2004. Since 2003, he has been with the Radio Laboratory, TKK (Aalto University since 2010), first as a Research Assistant and later as a Researcher. His current research interests include radio channel measurements and modeling.

Pertti Vainikainen received the degree of Master of Science in Technology, Licentiate of Science in Technology and Doctor of Science in Technology from Helsinki University of Technology (TKK) in 1982, 1989 and 1991, respectively. From 1992 to 1993 he was Acting Professor of Radio Engineering, since 1993 Associate Professor of Radio Engineering and since 1998 Professor in Radio Engineering, all in the Radio Laboratory (since 2008 Department of Radio Science and Engineering)of TKK (since 2010 Aalto University). In 1993-97 he was the director of the Institute of Radio Communications (IRC) of TKK, and a visiting professor in 2000 at Aalborg University, Denmark and in 2006 at University of Nice in France. His main fields of interest are antennas and propagation in radio communications and industrial measurement applications of radio waves. He is the author or co-author of 6 books or book chapters and about 320 refereed international journal or conference publications and the holder of 11 patents.

Claude Oestges received the M.Sc. and Ph.D. degrees in Electrical Engineering from the Université catholique de Louvain (UCL), Louvain-la-Neuve, Belgium, respectively in 1996 and 2000. In January 2001, he joined as a post-doctoral scholar the Smart Antennas Research Group (Information Systems Laboratory), Stanford University, CA, USA. From January 2002 to September 2005, he was associated with the Microwave Laboratory UCL as a post-doctoral fellow of the Belgian Fonds de la Recherche Scientifique (FRS). Claude Oestges is presently a FRS Research Associate and Assistant Professor at UCL. He is the author or co-author of one book and more than 120 research papers and communications, and was the recipient of the 1999-2000 IET Marconi Premium Award and of the 2004 IEEE Vehicular Technology Society Neal Shepherd Award.